I&EC research
Industrial & Engineering Chemistry Research
pubs.acs.org/IECR
Article

Combined GCMC, MD, and DFT Approach for Unlocking the Performances of COFs for Methane Purification

Omer Faruk Altundal, Zeynep Pinar Haslak, and Seda Keskin*

Cite This: *Ind. Eng. Chem. Res.* 2021, 60, 12999−13012

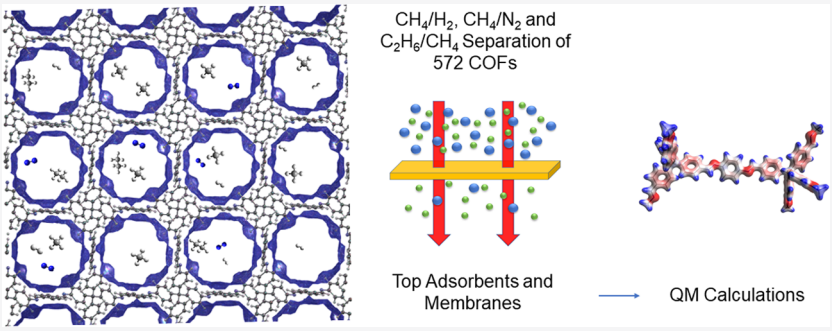

ABSTRACT: Covalent organic frameworks (COFs) are promising materials for gas storage and separation; however, the potential of COFs for separation of CH_4 from industrially relevant gases such as H_2, N_2, and C_2H_6 is yet to be investigated. In this work, we followed a multiscale computational approach to unlock both the adsorption- and membrane-based CH_4/H_2, CH_4/N_2, and C_2H_6/CH_4 separation potentials of 572 COFs by combining grand canonical Monte Carlo (GCMC) and molecular dynamics (MD) simulations and density functional theory (DFT) calculations. Adsorbent performance evaluation metrics of COFs, adsorption selectivity, working capacity, regenerability, and adsorbent performance score were calculated for separation of equimolar CH_4/H_2, CH_4/N_2, and C_2H_6/CH_4 mixtures at vacuum swing adsorption (VSA) and pressure swing adsorption (PSA) conditions to identify the best-performing COFs for each mixture. Results showed that COFs could achieve selectivities of 2−85, 1−7, and 2−23 for PSA-based CH_4/H_2, CH_4/N_2, and C_2H_6/CH_4 separations, respectively, outperforming conventional adsorbents such as zeolites and activated carbons for each mixture. Structure−performance relations revealed that COFs with pore sizes <10 Å are promising adsorbents for all mixtures. We identified the gas adsorption sites in the three top-performing COFs commonly identified for each mixture by DFT calculations and computed the binding strength of gases, which were found to be on the order of C_2H_6 > CH_4 > N_2 > H_2, supporting the GCMC results. Nucleus-independent chemical shift (NICS) indexes of aromaticity for adsorption sites were calculated, and the results revealed that the degree of linker aromaticity could be a measure for the selection or design of highly alkane-selective COF adsorbents over N_2 and H_2. Finally, COF membranes were shown to achieve high H_2 permeabilities, 4.57×10^3−1.25×10^6 Barrer, and decent membrane selectivities, as high as 4.3, outperforming polymeric and MOF-based membranes for separation of H_2 from CH_4.

1. INTRODUCTION

Natural gas, as one of the main energy resources, is gaining more and more attention due its clean energy supply compared to other types of fossil fuels. Natural gas is mostly composed of methane; however, it also contains some impurities such as hydrogen, nitrogen, carbon dioxide, and long-chain hydrocarbons depending on its source. These impurities either decrease the energy density of the natural gas or increase the CO_2 emission of natural gas; thus, removal of the contaminants from methane prior to its utilization in energy applications is crucial.[1,2] Methods like pressure swing adsorption (PSA) and vacuum swing adsorption (VSA) have been widely used for the purification of natural gas.[3−5] Traditional porous materials like zeolites and activated carbons have been used as adsorbents for selective separation of methane from other gases; however, they mostly suffer from low selectivities and low adsorption capacities.[6,7] Thus, there is an ongoing search for new materials with promising adsorption properties.

Metal−organic frameworks (MOFs) are crystalline porous materials in which metallic nodes are connected to each other with organic ligands.[8] Due to the vast number of available metallic nodes and organic ligands, MOFs have diverse physical and chemical properties such as variable surface

Received: May 7, 2021
Revised: August 10, 2021
Accepted: August 10, 2021
Published: August 25, 2021

https://doi.org/10.1021/acs.iecr.1c01742
Ind. Eng. Chem. Res. 2021, 60, 12999−13012

areas and porosities, which can be tuned by in situ or post-synthesis modifications to achieve the best-performing materials for a specific application.[9−11] MOFs have been considered as promising materials for both adsorption- and membrane-based CH_4 separation from various gases.[12−16] Since the number of experimentally synthesized MOFs and MOF-like materials has reached ∼100 000, identifying the best possible material for a specific gas separation using purely experimental manners is not practical.[17] Thus, high-throughput computational screening (HTCS) methods have been utilized to assess the adsorption-based CH_4/H_2, CH_4/N_2, CO_2/CH_4, C_2H_6/CH_4, and C_3H_8/CH_4 separation performances of MOFs.[18−22] A total of 4350 MOFs were studied for CH_4/H_2 mixture separation at VSA and PSA conditions, and CH_4/H_2 selectivities of MOFs were predicted based on the porosity and the largest cavity diameter (LCD) of MOFs, and the difference between the heat of adsorption values of gases (ΔQ_{st}) in MOFs.[23] Yan et al.[24] used molecular simulations to examine CH_4/N_2 mixture separation potentials of 5109 MOFs and revealed that MOFs with pore-limiting diameters (PLDs) in the range of 3.8−4.7 Å achieve high selectivities. Borah and Ponraj screened about 12 000 MOFs for C_2H_6/CH_4 separation and highlighted that MOFs with the Zr^{4+} cation are promising candidates for purification of CH_4.[25] MOFs have also been investigated for membrane-based CH_4/C_2H_6 and CH_4/H_2 separations,[26,27] and all of these works have highlighted the high potential of MOFs for CH_4 purification.

Covalent organic frameworks (COFs) have recently been considered as an emerging class of porous materials and have become alternatives to MOFs with their immense chemical and thermal stabilities due to the strong covalent bonds holding the structure, low densities, high porosities, and high gas separation performances.[28−30] Studies for the design of new COFs have gained pace, and the number of experimentally synthesized COFs is rapidly growing. COFs are composed of light elements, such as hydrogen, nitrogen, carbon, oxygen, and boron.[30−32] COFs, especially three-dimensional (3D) ones, offer higher surface areas and a higher number of adsorption sites than MOFs.[33] Similar to MOFs, structural properties of COFs can be tuned using in situ or post-synthetic modifications, granting the materials a diverse range of structural features.[28] Cao and Yang investigated the effect of Li doping on CH_4/H_2 separation performance of four different COFs using molecular simulations and showed that Li doping significantly increases the adsorption selectivity of COFs.[34] Tong et al.[35] screened 46 COFs to assess their CH_4/H_2, CO_2/H_2, and CO_2/CH_4 separation performances at PSA conditions and revealed that COFs can achieve higher selectivities (>100) and working capacities (>3 mol/kg) than zeolites and common MOFs.

The establishment of a computation-ready experimental COF (CoRE COF) database,[36] which currently consists of 449 solvent-free COF structures, promoted the utilization of HTCS for COFs.[37] Yan et al.[37] studied CO_2/CH_4 separation performance of 290 functionalized CoRE COF membranes at 10 bar, 298 K, and showed that 137 of them could outperform traditional polymers for CO_2/CH_4 separation. Ongari et al.[38] created the CURATED (Clean, Uniform, and Refined with Automatic Tracking from Experimental Database) COF database consisting of 324 structures with high-quality partial charges. They screened the CURATED COFs[38] along with the hypothetical COFs[39] for CO_2/N_2 separation and reported that many of the COFs have lower parasitic energies than the amine scrubbing process, which is conventionally used for CO_2 capture. Our group recently screened 295 COFs for CO_2/N_2 separation at VSA, PSA, and TSA conditions and reported that COFs with pore sizes < 10 Å, 0.6 < porosity < 0.8, and surface area < 4500 m^2/g are the most promising candidates for flue gas separation.[40] A total of 288 COFs were studied using HTCS methods for CO_2/H_2 separation at five different operating conditions, and COFs with narrow pores and low porosities were identified as the best-performing candidates for CO_2 separation from H_2.[41]

As evidenced from this literature review, COFs have been extensively studied for CO_2-related separations including CO_2/N_2, CO_2/H_2, and CO_2/CH_4, but we still have very limited information about the CH_4 separation potentials of COFs from other gases such as H_2, N_2, and C_2H_6. Motivated by this, we used an HTCS approach combining grand canonical Monte Carlo (GCMC) and molecular dynamics (MD) simulations to unlock the potential of COFs for adsorption- and membrane-based CH_4 separation from H_2, N_2, and C_2H_6. First, we performed GCMC simulations for the experimentally reported 572 COFs to compute equimolar CH_4/H_2, CH_4/N_2, and C_2H_6/CH_4 mixture adsorption properties of COFs at VSA and PSA conditions. Using this adsorption data, various adsorbent evaluation metrics were computed, and COFs were ranked according to these metrics to identify the top 10 materials for each separation process. The common top adsorbents for the three gas separation processes were studied in detail by performing density functional theory (DFT) calculations to understand the underlying gas adsorption dynamics. Adsorption-based CH_4 separation performances of COFs were compared with those of MOFs and zeolites to reveal their potential. Relations between structural properties and gas separation performances of COFs were examined to describe the best combination of structural characteristics leading to the most promising COF adsorbents for separation of each gas mixture. We finally computed membrane-based CH_4/H_2, CH_4/N_2, and C_2H_6/CH_4 separation performances of COFs by performing MD simulations. Gas permeability and selectivity of COF membranes were compared with those of MOF membranes and conventional polymer membranes. Our results will be useful in (i) providing a comparison between CH_4 purification performances of COFs with those of MOFs, zeolites, and polymers; (ii) highlighting the most promising COFs for CH_4 separation from various gases to guide the future experimental studies; and (iii) contributing to the design of new and novel COFs with greater potentials for CH_4 purification than existing COFs.

2. COMPUTATIONAL DETAILS

We used the CURATED COF[38] database, which consists of 598 distinct COF structures. The physical properties of COFs such as PLD, LCD, porosity (ϕ), accessible surface area (S_{acc}), and density were computed using Zeo++ software.[42] A probe radius of 1.86 Å (kinetic radius of the N_2 molecule) was employed for the calculations of surface area, and the COFs with zero S_{acc} were eliminated so that the gas molecules studied in this work can adsorb into the remaining COFs. CH_4/H_2, CH_4/N_2, and C_2H_6/CH_4 mixtures were assumed to be equimolar as most of the experimental studies in the literature that we compared our results with consider equimolar mixtures.[43,44] Moreover, Guo et al.[45,46] recently showed that composition does not significantly change the simulated C_2H_6/CH_4 and CH_4/H_2 selectivities of ZIFs. To compute the

https://doi.org/10.1021/acs.iecr.1c01742
Ind. Eng. Chem. Res. 2021, 60, 12999−13012

mixture adsorption data in COFs, such as gas uptakes (N) and isosteric heat of adsorption (Q_{st}), we performed GCMC simulations using the RASPA simulation code.[47] The fluctuation method[48] was employed to calculate Q_{st} values of gases, and the difference between the isosteric heats of adsorption of gases (ΔQ_{st}) was computed by subtracting the Q_{st} value of the weakly adsorbed gas molecule from the Q_{st} value of the strongly adsorbed gas molecule in a mixture.

Two different operating conditions were considered. In VSA (PSA) conditions, the adsorption pressure was set to 1 bar (10 bar), while the desorption pressure was set to 0.1 bar (1 bar). The temperature was fixed at 298 K for both operating conditions. Pressure-to-fugacity conversion was utilized using the Peng−Robinson equation of state.[49] The non-bonded interactions were defined with the Lennard-Jones (LJ) 12−6 potential, and a cutoff radius of 14 Å was employed for the truncation of those interactions.[50] The number of unit cells for COFs was adjusted so that the dimension of the simulation box is at least twice that of the cutoff distance. Electrostatic interactions, which were defined by the Coulomb potential,[51] were considered for the separation of the CH_4/N_2 mixture since the N_2 molecule has a quadrupole moment. COFs in the CURATED database were reported with high-quality density-derived electrostatic and chemical (DDEC) charges, and these charges were used in the calculations of electrostatic interactions between N_2 and COF atoms. The Ewald summation was used for the long-range interactions.[52] A total of 10 000 and 20 000 cycles were set for initialization and taking ensemble averages of GCMC simulations, respectively. The H_2 molecule was modeled as a single-site LJ 12−6 potential, and its potential parameters were taken from the Buch model.[53] CH_4 and C_2H_6 molecules were modeled using the united atom model of the TraPPE force field,[54] where CH_4 was modeled as a single-site spherical LJ 12−6 potential and C_2H_6 was modeled as a two-site LJ 12−6 potential.[55] A three-site model was employed for N_2 where two N atoms are residing on the sides and partial charges are at the center of mass.[56] Potential parameters of COF atoms were taken from the DRIEDING force field[57] since a good agreement between simulated and experimentally reported CO_2 isotherms of COFs was found in our previous works.[40,41] A good agreement between simulations and experimentally measured CH_4 adsorption isotherms of COFs[58] is also seen in Figure S1 of the Supporting Information (SI). Using the results obtained from GCMC simulations, we calculated various adsorbent performance evaluation metrics including adsorption selectivity (S_{ads}), working capacity (ΔN), adsorbent performance score (APS), and percent regenerability (R%), as listed in Table 1.

The quantitative analyses of CH_4, C_2H_6, N_2, and H_2 interactions with the three common top COFs for C_2H_6/CH_4, CH_4/N_2, and CH_4/H_2 separations were performed using DFT calculations. Cluster models were generated to represent the linkers of these three common top COFs. To mimic the constrained environment of the COFs, selected key atoms in cluster models were kept frozen in their crystalline positions, and the rest of the atoms were allowed to be fully optimized. All possible conformations of the COF−gas pairs were located with the Becke−three-parameter-Lee−Yang−Parr (B3LYP)[59,60] functional including Grimme's D2 correction[61] employing the all-electron 6-31G* basis set using the Gaussian09[62] program package. The vibrational frequency calculations were performed to ensure that no imaginary frequency remained. The binding energies between the gases and the COFs were calculated using $\Delta E_{bind} = E_{COF+Gas} - (E_{COF} + E_{Gas}) + \delta^{BSSE}$, where $E_{COF+Gas}$ is the energy of the COF−gas complex, E_{COF} and E_{Gas} denote the COF and gas energies, respectively, and δ^{BSSE} is the basis set superposition error correction employed by the Counter Poise approach. The magnetic properties of the COFs were calculated by the gauge-independent atomic orbital (GIAO) method with the 6-31+G** basis set.

Table 1. Calculation of Metrics Used to Assess Adsorption- and Membrane-Based Gas Separation Performances of COFs[a]

metrics	formula
adsorption selectivity	$S_{ads,i/j} = \frac{N_{ads,i}}{N_{ads,j}} \times \frac{y_j}{y_i}$
working capacity (mol/kg)	$\Delta N_i = N_{ads,i} - N_{des,i}$
adsorbent performance score (mol/kg)	$APS = S_{ads,i/j} \times \Delta N_i$
percent regenerability	$R\% = \frac{\Delta N_i}{N_{ads,i}} \times 100\%$
diffusion selectivity	$S_{diff,i/j} = \frac{D_{self,i}}{D_{self,j}}$
membrane selectivity	$S_{mem,i/j} = S_{ads,i/j} \times S_{diff,i/j}$
permeability (Barrer)	$P_i = \frac{c_{i,ads} \times D_{self,i}}{f_i}$

[a] i: Selected component, CH_4 for CH_4/H_2 and CH_4/N_2 mixtures, C_2H_6 for the C_2H_6/CH_4 mixture. N_{ads} (mol/kg): Gas uptake at adsorption conditions. N_{des} (mol/kg): Gas uptake at desorption conditions. y: Composition of the gas species in the bulk phase. f (Pa): Partial pressure of gas species in the mixture. c (mol/m^3): Gas loading obtained from GCMC simulations. D (m^2/s): Self-diffusivity of gas obtained from MD simulations. 1 Barrer = 3.348×10^{-16} mol·m/(m^2·s·Pa).

MD simulations were performed for 3×10^6 cycles in the NVT ensemble to compute the self-diffusivities of CH_4, H_2, N_2, and C_2H_6 gases in COFs. A total of 5×10^5 cycles were set for both initialization and equilibration of NVT-MD simulations, where the Nosé−Hoover thermostat was employed.[63] The slope of mean-square displacements of gases was used to calculate the self-diffusivities by the Einstein equation.[64] All COFs were assumed to be rigid to save computational time. Since the pore apertures of the COF structures in this study are larger than the kinetic diameters of the gas molecules, the results of our molecular simulations are not expected to be affected by the flexibility of the structures.[27] The gas loadings computed with GCMC simulations at 1 bar and 298 K were taken as the number of gas molecules in the simulation box for NVT-MD simulations to calculate the self-diffusivities of gases through the pores of COFs. Gas permeabilities (P), diffusion selectivities (S_{diff}), and membrane selectivities (S_{mem}) were computed as shown in Table 1. We performed MD simulations for all of the COFs for membrane-based CH_4/H_2 mixture separation and identified the top 10 membranes based on their permeabilities and selectivities. Considering the expense of MD simulations, only these top 10 COF membranes were studied for membrane-based separation of CH_4/N_2 and C_2H_6/CH_4 mixtures.

https://doi.org/10.1021/acs.iecr.1c01742
Ind. Eng. Chem. Res. 2021, 60, 12999−13012

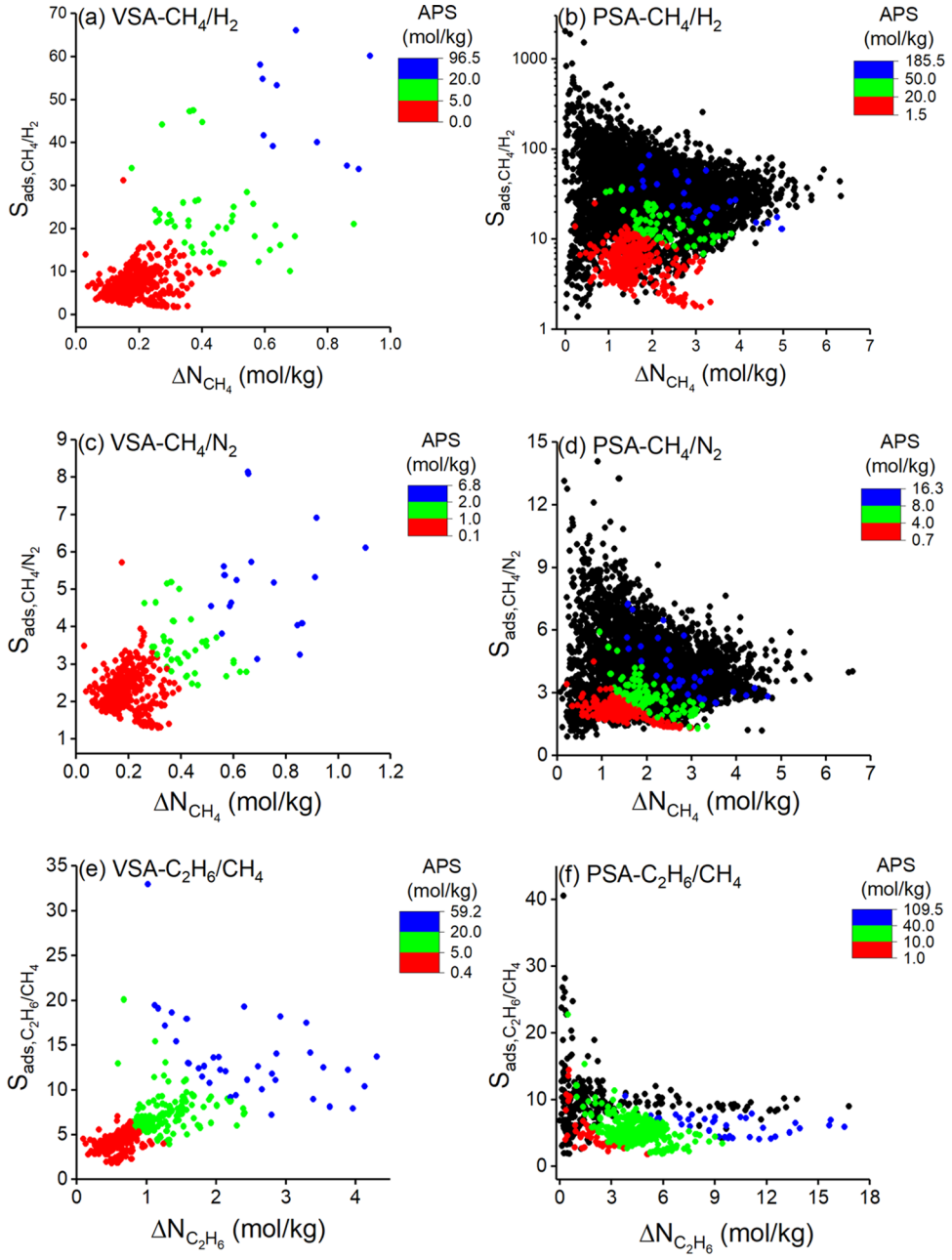

Figure 1. Selectivity and working capacity of 572 COFs for separation of (a, b) CH_4/H_2: 50/50 mixture, (c, d) CH_4/N_2: 50/50 mixture, and (e, f) C_2H_6/CH_4: 50/50 mixture at VSA (1−0.1 bar at 298 K) and PSA (10−1 bar at 298 K) conditions. Colors represent APSs of COFs. MOFs from our previous works[21,23,66] (black data points, 4350 MOFs for CH_4/H_2, 4738 MOFs for CH_4/N_2, and 281 MOFs for C_2H_6/CH_4 separations) were included in (b), (d), and (f) for comparison.

3. RESULTS AND DISCUSSION

First, we analyzed adsorption-based CH_4 separation performances of 572 COFs. Figure 1 shows the adsorption selectivity (S_{ads}) of COFs as a function of their working capacities (ΔN) for CH_4/H_2, CH_4/N_2, and C_2H_6/CH_4 mixture separations at VSA and PSA conditions. In CH_4/H_2 and CH_4/N_2 mixtures, CH_4 interacts more strongly with the framework than H_2 and N_2, making all COFs CH_4-selective adsorbents. Thus, we reported the selectivities and working capacities based on CH_4 for CH_4/H_2 and CH_4/N_2 separations. On the other hand, for the C_2H_6/CH_4 mixture, selectivities and working capacities were reported based on C_2H_6 since the two site-represented C_2H_6 molecules were more strongly adsorbed into COFs than the single sited-CH_4. $S_{ads,CH_4/H_2}$ values of COFs were calculated to be in the ranges of 2−102 and 2−85 at VSA and PSA conditions, respectively. Higher selectivities were observed for COFs at VSA conditions compared to PSA conditions for CH_4/H_2 separation, as shown in Figure 1a,b, which can be attributed to the packing effects favoring adsorption of the smaller molecule at higher pressures.[65] ΔN_{CH_4} values of COFs at VSA conditions were between 0.03 and 1.15 mol/kg, whereas at PSA conditions, higher values, 0.22−4.97 mol/kg, were observed. These higher working capacities were the result of higher gas uptakes achieved at PSA conditions.

A promising adsorbent for gas separation applications should achieve the combination of high selectivity and high working

https://doi.org/10.1021/acs.iecr.1c01742
Ind. Eng. Chem. Res. 2021, 60, 12999−13012

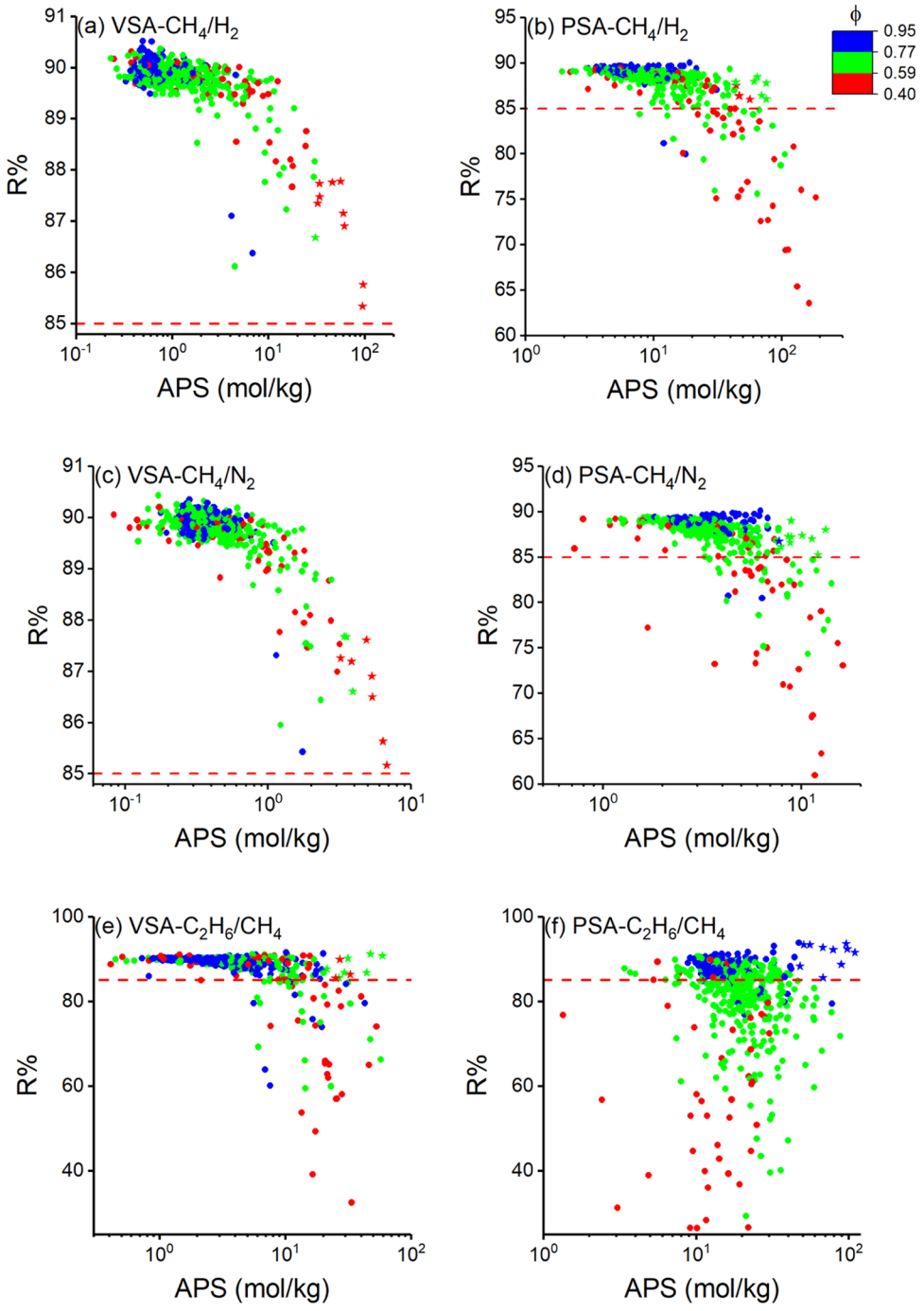

Figure 2. *R*% and APSs of 572 COFs for separation of (a, b) CH_4/H_2 mixture, (c, d) CH_4/N_2 mixture, and (e, f) C_2H_6/CH_4 mixture at VSA and PSA conditions. Colors represent the porosity of COFs, and stars represent the top 10 COFs identified for each condition. Red dashed line represents the *R*% = 85% line.

capacity.[67] Therefore, we calculated the APS of COFs, the multiplication of S_{ads} and ΔN, to assess the gas separation performances of COFs and presented with the color scale in Figure 1a,b. Higher ΔN_{CH_4} values were obtained for COFs at PSA conditions rather than at VSA conditions, whereas there was no significant difference between the selectivities achieved at VSA and PSA conditions. Therefore, higher APSs were obtained at PSA conditions. These results suggest that using COFs in PSA-based CH_4/H_2 separation would be more efficient than VSA-based separation. The COFs with the highest APS at PSA conditions mostly have lower ΔN_{CH_4} compared to other COFs. Therefore, for CH_4/H_2 separation, S_{ads} has a more pronounced impact than ΔN to achieve a high APS in the PSA process. Similar results were obtained for CH_4/N_2 separation at PSA and VSA conditions in Figure 1c,d. Due to the higher ΔN_{CH_4} values achieved at PSA conditions (0.03−1.10 mol/kg at VSA, 0.21−4.70 mol/kg at PSA), APSs of COFs were higher than those at VSA conditions; thus, PSA can be considered as a desirable condition for CH_4/N_2 separation.

The largest difference between the performances of COFs for CH_4/H_2 and CH_4/N_2 separations was observed in the

https://doi.org/10.1021/acs.iecr.1c01742
Ind. Eng. Chem. Res. 2021, 60, 12999−13012

selectivities. S_{ads} values of COFs were between 2 and 85 for PSA-based CH_4/H_2 separation, whereas S_{ads} values of COFs were in the range of 1−7 for CH_4/N_2 separation at the same conditions. To investigate this difference, in Figure S2, we analyzed the ΔQ_{st} values of mixtures, which can be related to selectivities of materials.[68,69] We observed that $\Delta Q_{st,CH_4/H_2}$ values of COFs (2.72−17.14 kJ/mol) are always higher than $\Delta Q_{st,CH_4/N_2}$ values (1.14−6.42 kJ/mol), leading to lower selectivities for the CH_4/N_2 mixture. This can be explained by two reasons: (i) LJ energy parameter of N_2 is larger than that of H_2, which leads to larger LJ interactions between COF atoms and N_2 molecules; and (ii) N_2 molecules have electrostatic interactions with the COF atoms, which are absent for H_2 molecules. Thus, the competition between N_2 and CH_4 is stronger compared to H_2 and CH_4, leading to lower selectivities for the CH_4/N_2 mixture. To better understand which of these interactions contribute more to the adsorption of the N_2 molecule, we switched off the Coulombic interactions between COF atoms and N_2 molecules and reperformed GCMC simulations. S_{ads} values of COFs computed with and without considering the Coulombic interactions between COFs and N_2 are presented in Figure S3. $S_{ads,CH_4/N_2}$ values do not significantly change when the electrostatic interactions were neglected, which can be attributed to the absence of strong metal atoms in COFs.[38,40] Therefore, we concluded that LJ interactions are the main contributors to the adsorption of N_2 molecules in COFs.

In Figure 1e,f, selectivities and working capacities of COFs for separation of CH_4 from C_2H_6 are shown at VSA and PSA conditions, respectively. $S_{ads,C_2H_6/CH_4}$ ($\Delta N_{C_2H_6}$) values of COFs at VSA and PSA conditions were computed as 2−33 and 2−23 (0.1−4.3 and 0.3−16.5 mol/kg), respectively. COFs have slightly lower selectivities at PSA conditions than VSA conditions; however, the high $\Delta N_{C_2H_6}$ achieved by COFs at PSA conditions outweighs their selectivities, resulting in higher APSs for COFs at PSA conditions. Contrary to the CH_4/H_2 mixture, the COFs with the highest APSs were identified to have high $\Delta N_{C_2H_6}$. Thus, it can be concluded that ΔN has a greater importance than S_{ads} for COFs to achieve high APSs for C_2H_6/CH_4 separation.

We also included S_{ads} and ΔN values of MOFs that we computed in our previous works[21,23] in Figure 1b,d,f to compare the separation performance of COFs with that of MOFs. CH_4/H_2 selectivities of MOFs at PSA conditions were between 1 and 2028, which are significantly higher than the most selective COF investigated in this study (CTF-FUM, S_{ads}: 85.3). The lower CH_4/H_2 selectivity of COFs compared to MOFs can be attributed to the larger pore apertures of COFs, which allow both gases to be adsorbed inside pores. Of the COFs used in this work, 80% have PLD > 10 Å, while this ratio was only 5% for MOFs. However, ΔN_{CH_4} values of MOFs (0.01−7.27 mol/kg) are comparable to those of COFs (0.22−4.97 mol/kg). Still, MOFs outperform COFs for adsorption-based CH_4/H_2 separation due to their high selectivities. Selectivities and ΔN_{CH_4} of COFs (1−7; 0.2−4.7 mol/kg) are comparable to those of MOFs (1−14; 0.1−6.6 mol/kg) for PSA-based CH_4/N_2 separation. This is due to the similarity in the physical features of both gases limiting the CH_4/N_2 mixture selectivity.[24] Nevertheless, APSs of MOFs (0.2−30.7 mol/kg) are slightly higher than those of COFs (0.7−16.2 mol/kg). Still, COFs can be used as alternative adsorbents because they show better stabilities than MOFs under harsh chemical conditions, which may make COFs preferable for practical applications over MOFs.[28] Similar results were obtained for PSA-based C_2H_6/CH_4 separation, as shown in Figure 1f, where APSs of MOFs (0.4−150.5 mol/kg) are slightly higher than APSs of COFs (1.4−109.4 mol/kg); however, COFs can be good alternatives to MOFs.

Regenerability (R%) should be considered in the selection of the top materials for cyclic VSA and PSA processes since materials offering high APSs usually have low R% values.[70,71] Calculated R% values of COFs as a function of their APSs are given in Figure 2a,b for CH_4/H_2, in Figure 2c,d for CH_4/N_2, and in Figure 2e,f for C_2H_6/CH_4 separation at VSA and PSA conditions, respectively. We set a desired value, R% > 85% (red dotted line), to easily identify the promising COFs. For CH_4/H_2 and CH_4/N_2 mixtures, all of the COFs are over the R% > 85% line at VSA conditions, as shown in Figure 2a,c. This is because of the low amount of adsorbed gas in the pores at low pressure, which can easily desorb at 0.1 bar. However, as the pressure increases, gases prefer to remain inside the pores, especially for COFs with lower porosities, due to the strong confinement inside the narrow pores.[72] Therefore, R% values of COFs at PSA conditions are lower than those at VSA conditions (Figure 2b,d). Although most of the COFs could still surpass the R% > 85% target at PSA conditions, COFs offering the best APSs are under the R% > 85 line and are unfeasible for use in practical applications. This trend was previously observed for COFs in adsorption-based CO_2/N_2 separation.[40] For example, a COF (CTF-FUM) could be a top material for both CH_4/H_2 and CH_4/N_2 separations due to its high APS (85.3 mol/kg for CH_4/H_2, 11.7 mol/kg for CH_4/N_2) at PSA conditions; however, its R% values were calculated as 64 and 61%, respectively, making the material inefficient for a cyclic adsorption process. R% values of COFs are generally lower for C_2H_6/CH_4 separation compared to CH_4/H_2 and CH_4/N_2 separations, as shown in Figure 2e,f. This is due to the stronger adsorption of C_2H_6, which decreases the R%. Similar to other mixtures, low R% values were observed for COFs with the highest APSs for C_2H_6/CH_4 at VSA conditions. Interestingly, this trend changed in PSA conditions, where R% of COFs increases directly proportional to their APSs. This can be attributed to the dominance of $\Delta N_{C_2H_6}$ in the assessment of APS of COFs for PSA-based C_2H_6/CH_4 separation as discussed before. The COFs with the highest APSs for PSA-based C_2H_6/CH_4 separation have the highest porosities leading to high $\Delta N_{C_2H_6}$ and R% values. Thus, COFs can achieve a combination of high APSs with high R% values for PSA-based C_2H_6/CH_4 separation.

We identified the top 10 promising COF adsorbents for each gas separation and condition by ranking the materials based on their APSs and focusing on the ones having R% > 85%. The 3D structural representations of the top COF adsorbents, shown with stars in Figure 2, are given in Figure S4, and their performance metrics are given in Tables S1−S3, along with the selectivities and working capacities of some representative conventional adsorbents for the comparison of COFs with industrially relevant materials. For PSA-based CH_4/H_2 and CH_4/N_2 separations and VSA-based C_2H_6/CH_4 separation, COF-303 was identified to be the most promising adsorbent. COF-303 has a small pore size (LCD of 8.31 Å) relative to other COFs and low S_{acc} (1821 m^2/g) leading to

https://doi.org/10.1021/acs.iecr.1c01742
Ind. Eng. Chem. Res. 2021, 60, 12999−13012

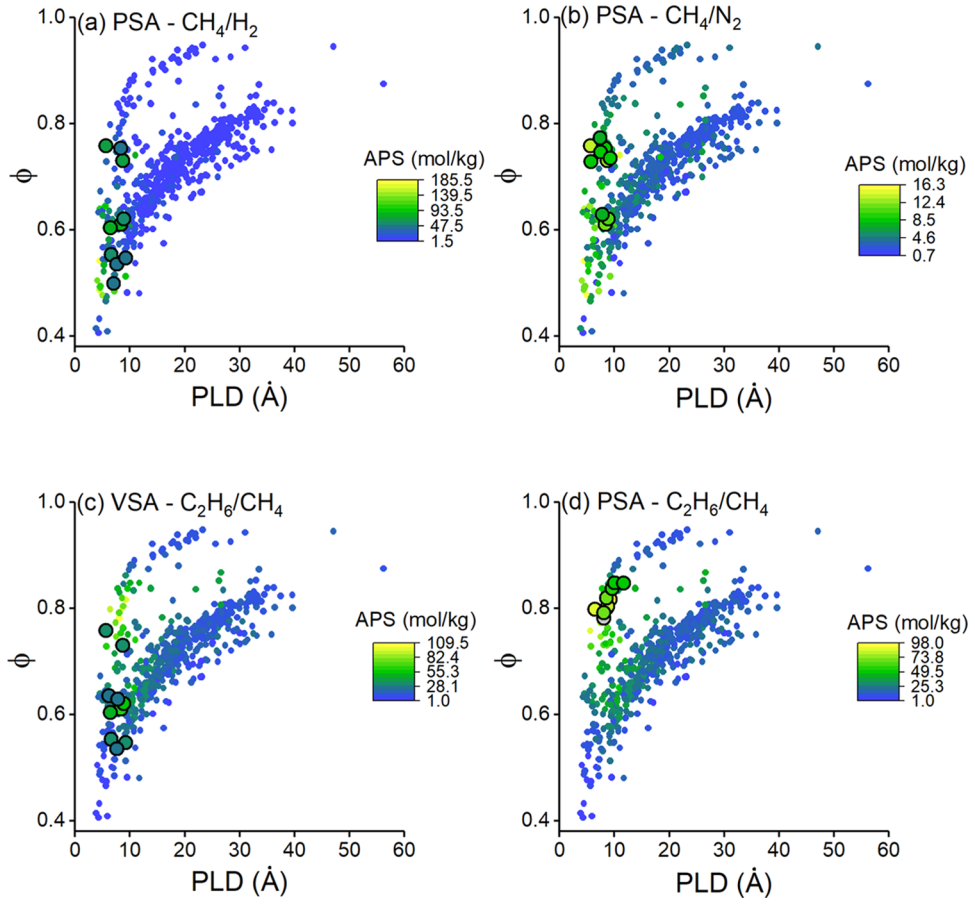

Figure 3. PLDs and porosities of 572 COFs as a function of their APSs calculated for (a) CH_4/H_2 and (b) CH_4/N_2 separation at PSA conditions, and (c, d) C_2H_6/CH_4 separation at VSA and PSA conditions. Big circles with thick edges represent the top 10 COFs identified for each mixture at each condition.

high selectivities. For PSA-based C_2H_6 separation, the most promising COF candidate was identified as COF-102, which has a high porosity (0.78) and high S_{acc} (5049 m^2/g) resulting in a high working capacity. Both COF-303 and COF-102 were reported to have excellent stabilities; thus, they can be ideal materials for utilization in practical applications.[33,73] Most of the top COF candidates identified for CH_4/H_2 separation have higher S_{ads} and ΔN values than commercial adsorbents. For example, $S_{ads,CH_4/H_2}$ of commercial zeolite 13X is 22 at 1 bar and 308 K, while its ΔN_{CH_4} is 0.32 mol/kg.[74] Selectivity and working capacity of the top COFs for VSA-based CH_4/H_2 separation were in the ranges of 40−102 and 0.59−1.15 mol/kg, respectively. Similar results were obtained for COFs when CH_4/N_2 and C_2H_6/CH_4 separations were considered. For instance, selectivity and working capacity of the top COFs (4.1−8.2 and 0.6−1.1 mol/kg, respectively) identified for VSA-based CH_4/N_2 separation were higher than those of Linde 4A ($S_{ads,CH_4/N_2}$: 3.4 and ΔN_{CH_4}: 0.4 mol/kg for an equimolar mixture) measured at 1 bar and 302 K.[75] Also, the top COFs identified for VSA-based C_2H_6/CH_4 separation achieved higher selectivities and working capacities than zeolite CaX (ideal selectivity: 5; $\Delta N_{C_2H_6}$: 0.9 mol/kg) at the same conditions.[76] Thus, these results suggest that COFs can outperform conventional adsorbents for the purification of CH_4 from H_2, N_2, and C_2H_6.

We then examined the relation between the structural properties of 572 COF adsorbents and their gas separation performances to highlight the best combination of structural features. Figure 3 shows the APSs of COFs as a function of their PLDs and porosities for CH_4/H_2, CH_4/N_2, and C_2H_6/CH_4 mixture separations at PSA conditions. Results for CH_4/H_2 and CH_4/N_2 mixtures at VSA conditions are given in Figure S5. APSs increase with a decrease in PLDs of COFs for all mixtures at all conditions. As the pore aperture becomes smaller, selectivity increases in favor of the strongly adsorbed gas.[72] As a result, the top COFs identified for each separation have PLDs < 10 Å, except for C_2H_6/CH_4 separation at PSA conditions in which ΔN is the dominating factor in APSs of COFs as discussed earlier. Changes in porosity have two different effects on the adsorption properties of COFs: a decrease in porosity may (i) lead to an increase in selectivities of COFs due to the stronger confinement of gases, and (ii) result in an increase in working capacities of COFs due to higher gas uptakes. For PSA-based CH_4/H_2 separation and VSA-based C_2H_6/CH_4 separation, APSs are negatively correlated with COFs' porosities since S_{ads} is the dominant factor in the assessment of APSs for these separations. Therefore, most of the top COFs have porosity < 0.6. On the other hand, ΔN is the dominating factor for the assessment of APSs in PSA-based C_2H_6/CH_4 separation, and porosity is positively correlated with APSs. Thus, COFs with high porosities, >0.8, are identified as the most promising materials.

Among the top COFs identified for each mixture, COF-303, COF-300, and PZ-COF2 are common for PSA-based CH_4/H_2 and CH_4/N_2 separations and VSA-based C_2H_6/CH_4 separa-

https://doi.org/10.1021/acs.iecr.1c01742
Ind. Eng. Chem. Res. 2021, 60, 12999−13012

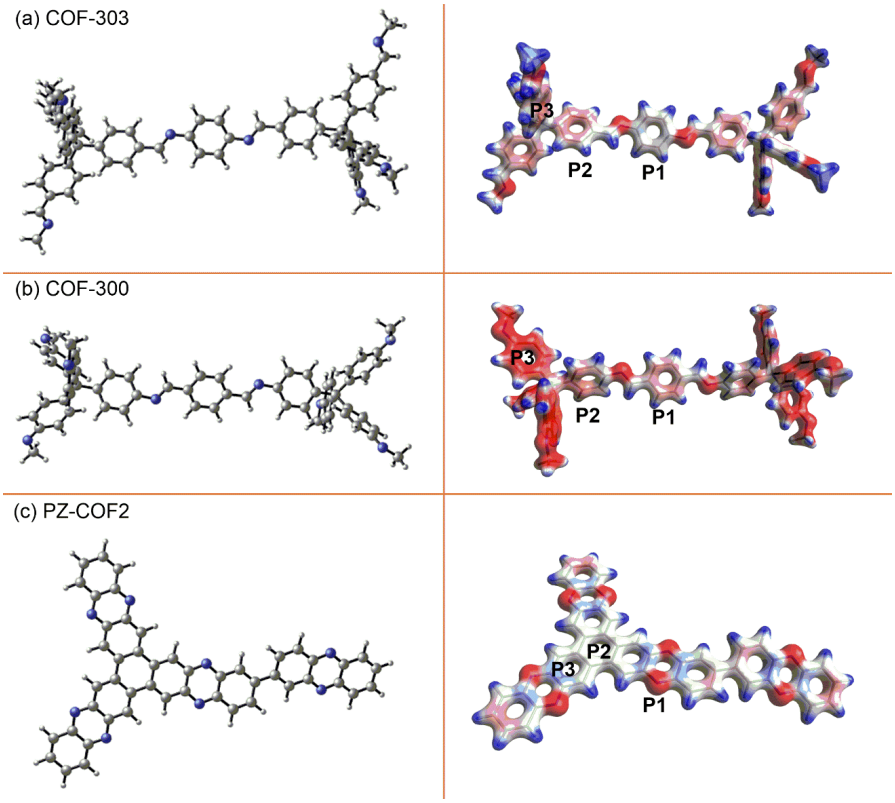

COF	Density (g/cm^3)	PLD (Å)	S_{acc} (m^2/g)	ϕ	Bond type	Topology
COF-303	0.74	8.31	1821.19	0.61	Imine	dia
COF-300	0.72	8.86	1934.06	0.62	Imine	dia
PZ-COF2	0.56	8.66	4393.09	0.73	Pyrazine	hcb

Figure 4. Three-dimensional representations and electrostatic potential maps of the linker fragments of the three common top COFs. White, hydrogen; gray, carbon; blue, nitrogen. Negative (positive) regions are depicted in red (blue) color.

Table 2. Calculated NICS(1) Values (ppm) for the Respective Linker Fragments and Calculated Binding Energies (kJ/mol) of the COF−Gas Pairs with Respect to the Positions of the Gases along with the Q_{st} (kJ/mol) of COF−Gas Pairs Obtained from GCMC Simulations[a]

			CH_4		C_2H_6		N_2		H_2	
	fragment	NICS(1)	E_{bind}	Q_{st}	E_{bind}	Q_{st}	E_{bind}	Q_{st}	E_{bind}	Q_{st}
COF-303	P1	−8.82	−5.30	−12.14	−11.10	−19.54	−5.63	−9.12	−0.06	−3.39
	P2	−9.19	−10.38		−15.99		−9.39		−0.62	
COF-300	P1	−8.83	−5.50	−11.56	−12.03	−18.46	−4.44	−8.59	0.55	−3.27
	P2	−8.94	−12.07		−21.05		−9.85		−0.72	
PZ-COF2	P1	−11.02	−7.12	−14.22	−9.82	−23.52	−5.23	−11.03	0.45	−3.52
	P2	0.40	−7.66		−14.99		−5.83		−0.20	
	P3	−9.11	−6.23		−14.99		−5.68		0.37	

[a]Negative signs of binding energies imply attractive interaction.

tion. Thus, these three common top materials were studied in detail by the DFT calculations. We prepared cluster models consisting of the organic linker fragments and optimized them in the presence of gas molecules. As an important tool for the interpretation of electrostatic interactions of a material with adsorbate molecules, electrostatic potential maps (ESPs) were generated and are presented in Figure 4 together with the 3D representations of the cluster models. All three COFs are composed of the same atoms, which differ in their arrangements in space. They have low PLDs (5.6−8.9 Å), leading to selective separation of gases and similar porosities (0.61−0.76). In COF-303, the repeating unit is the benzene-1,4-diamine double-bonded to phenyl groups by two amine ends. According to the ESP map, the most negative regions are located around conjugated N bonds, which act as good electron-donor sites. Aromatic rings, which are located at the linkers' joint, are also expected to exhibit good adsorption capability due to the electrostatic potentials generated. 1,4-phenylenedimethanimine scaffolds are bonded to phenyl groups by amine ends to form the linker fragments in COF-

https://doi.org/10.1021/acs.iecr.1c01742
Ind. Eng. Chem. Res. 2021, 60, 12999−13012

300. Electron-donating sites are located on the N atoms and the benzene rings. PZ-COF2 consists of phenazine scaffolds in which the most electronegative regions are concentrated on the N atoms, whereas the phenyl rings show less electronegativity.

From ESP maps, possible adsorption sites were determined and then the interactions between the gas molecules and the linker scaffolds were investigated to identify the most probable adsorption sites for each COF−gas pair. The binding energies for the COF−gas pair conformations were calculated, and the results are given in Table 2. To elucidate the relationship between the magnetic index of aromaticity of the rings and the stabilization of the gas molecules upon interaction, nucleus-independent chemical shift (NICS)[77,78] indexes were calculated for the linker fragments. Aromaticity of an organic or inorganic compound can be quantified by measuring the molecular magnetic response properties, such as chemical shifts, nuclear magnetic shieldings, and magnetic susceptibility, in the presence of an external magnetic field. The NICS method has been extensively employed for the evaluation of aromaticity, antiaromaticity, and nonaromaticity of ring systems, and it uses the induced current densities to quantify the aromaticity indices.[79−81] It is computed by introducing a dummy atom at the ring center (the average coordinates of the nonweighted heavy atoms) or at a certain distance below or above the ring, and then, the magnitude of the shielding constant is obtained. The negative value of the calculated absolute shielding at some point of the system is defined as NICS, and the more aromatic character of the ring corresponds to the more negative NICS value. It has been previously reported that NICS(1), which is obtained at 1 Å above the molecular plane, reflects the π-electron density better than NICS(0).[82] As presented in Table 2, the central phenyl fragment (P1) in COF-303 was calculated to be slightly less aromatic (−8.82 ppm) than the phenyl fragment in the edge (P2) (−9.19 ppm) due to the presence of two nitrogen atoms bonded to P1, which help in the conjugation of the π-electrons in the ring system through the imine bonds. This was confirmed by C_{ring}−N_{imide} (1.400 Å) and C_{ring}−C_{ring} (1.408 Å) distances of the P1 ring, which are almost equal, and C_{ring}−C_{imide} (1.460 Å) and C_{ring}−C_{ring} (1.403 Å) distances of the P2 fragment, which are not equal. All of the gases are adsorbed stronger by the more aromatic P2 site, as illustrated in Figure S6. Figure S6a displays that two hydrogens of CH_4 form C−H···π interactions with the center of masses of P2 and P3 rings, which are on the C_6 axis of benzene, and one hydrogen of CH_4 forms a H-bond with the electron-rich N atom of COF-303. The shorter C−H···π bond lengths (2.60 Å with P2 and 2.62 Å with P3) compared to the C−H···N bond (3.68 Å) indicate that the contribution of the C−H···π interaction to the stabilization of the CH_4 molecule is larger. Similar interactions are observed between COF-303 and C_2H_6, as shown in Figure S6b. C_2H_6 interacts slightly stronger with the P3 fragment (2.57 Å) than with the P2 fragment (2.78 Å), and the H-bond length of C−H···N is 2.81 Å, shorter than the C−H···N bond in COF-303-CH_4. This can be attributed to the larger polarizability of C_2H_6 (α = 4.226 Å^3),[83] which allows C_2H_6 to form stronger dispersion interactions with P3 compared to CH_4 (α = 2.448 Å^3),[83] and thus stronger adsorption of C_2H_6 (ΔE_{bind} = 15.99 kJ/mol) was observed with respect to CH_4 (ΔE_{bind} = 10.38 kJ/mol). Figure S6c displays the interactions between N_2 and COF-303. The internuclear axis of N_2 is oriented parallel to the C_6 axis of benzene rings at a distance of 3.23 Å above the P2 plane and 3.17 Å above the P3 plane, making an attractive quadrupole−quadrupole interaction. The lower polarizability of N_2 (α = 1.710 Å^3)[83] compared to C_2H_6 and CH_4 results in the formation of weaker dispersion forces with COF-303, and eventually weaker adsorption was observed (ΔE_{bind} = 9.39 kJ/mol). The geometrical representations of H_2 and COF-303, which are aligned to form the most favorable electrostatic interaction, are illustrated in Figure S6d. The interatomic distance between one H atom of H_2 and the center of mass of P2 is 2.78 Å and the other H atom of H_2 and the center of mass of P3 is 2.67 Å. H_2 is the least polarizable (α = 0.787 Å^3)[83] and the least adsorbed molecule by COF-303 among the gases considered in this study (ΔE_{bind} = 0.62 kJ/mol).

In COF-300, NICS assigns almost equal aromaticities to the P2 scaffold in the edge (−8.94 ppm) and the central P1 fragment (−8.83 ppm). The nitrogen atom bonded to P2 enriches the delocalized π-electron density in the ring system (C_{ring}−N_{imide} = 1.400 Å and C_{ring}−C_{ring} = 1.409 Å), but the tetrahedral carbon at the joint of the linkers does not take place in delocalization of the ring electrons (C_{ring}−C_{joint} = 1.524 Å). P1 is bonded to N atoms through doubly bonded carbon atoms (C_{ring}−C_{imide} = 1.461 Å and C_{ring}−C_{ring} = 1.408 Å). The interactions of the gases with COF-300 are very similar to their interactions with COF-303, as displayed in Figure S7a−d. All of the gas molecules are adsorbed stronger by P2 fragments (Table 2) due to the stronger electrostatic potential generated by the more electron-rich P2 and P3 scaffolds, as represented in Figure 4b. While the adsorption energies of N_2 and H_2 with COF-300 (9.85 and 0.72 kJ/mol, respectively) are very similar to their binding energies with COF-303, C_2H_6 and CH_4 are adsorbed strongly in COF-300 (21.05 and 12.07 kJ/mol, respectively) due to the presence of more electron-rich P2 and P3 regions in COF-300, as can be deduced from the ESP maps in Figure 4b. Since N_2 and H_2 have very low polarizabilities, they are not affected by the dispersion forces induced by P2 and P3 as much as C_2H_6 and CH_4.

While P1 and P3 fragments were calculated to be aromatic (−11.02 and −9.11 ppm) in PZ-COF2, the P2 fragment was determined as nonaromatic/antiaromatic (0.40 ppm). According to the binding energies given in Table 2, CH_4, N_2, and H_2 are adsorbed almost equally in P1, P2, and P3 regions, whereas C_2H_6 is adsorbed significantly stronger by P2−P3 fragments. CH_4 is stabilized on the P2 ring since it can form two C−H···π bonds with adjacent aromatic P3 rings at distances of 3.34 and 3.12 Å from the C_6 axis of P3 rings, as shown in Figure S8a. C_2H_6 is adsorbed stronger by PZ-COF2 (ΔE_{bind} = 14.99 kJ/mol) than CH_4 (ΔE_{bind} = 7.66 kJ/mol) since the former can form three C−H···π bonds with the adjacent P3 fragments as a result of its larger size and larger polarizability as discussed above and shown in Figure S8b. Similar to the interactions formed between N_2 and COF-300 and COF-303, the N_2 molecule's internuclear axis is oriented parallel to the C_6 axis of the P2 ring at a distance of 3.01 Å (Figure S8c). The almost equal binding energies calculated between N_2 and P1, P2, P3 regions, which possess different degrees of aromaticities, point out that adsorption of N_2 is not related to the aromatic/nonaromatic character of a ring. The same conclusion was valid for H_2 since the affinities of H_2 toward P1, P2, and P3 sites are very similar, as can be tracked from Table 2. Figure S8d illustrates the intermolecular interaction between the P2 ring of PZ-COF2 and H_2, which is driven by the weak van der Waals forces.

https://doi.org/10.1021/acs.iecr.1c01742
Ind. Eng. Chem. Res. 2021, 60, 12999−13012

The snapshots taken from GCMC simulations show that all of the gas molecules primarily occupy the P2 and P3 regions, as shown in Figure S9, in harmony with the DFT calculations. As shown in Table 2, although E_{bind} values between C_2H_6, CH_4, H_2, N_2 and COF-303, PZ-COF2, COF-300 obtained from the B3LYP-D2/6-31G* level are slightly different from the Q_{st} values calculated by GCMC simulations, adsorption strengths of the gases are on the order of C_2H_6 > CH_4 > N_2 > H_2 for all COFs, showing a good agreement with our GCMC simulations. Analysis of gas−COF pairs reveals that adsorption is mainly driven by the dispersion interactions between the COFs and gases, which are directly related to the polarizabilities of the molecules. On the other hand, as stated by Levitt and Perutz,[84] aromatic rings act as H-bond acceptors, and thus, C−H···π bonds formed between the linkers and C_2H_6 and CH_4 increase the strength of their adsorption. This was proven by comparing the binding energies calculated for each conformation of the gases with respect to their locations on P1, P2, and P3 regions of the COFs. Therefore, besides increasing the number of aromatic sites in a linker of COF, increasing the extent of aromaticity of the linker rings may result in stronger interactions and stronger adsorption of C_2H_6 and CH_4 in a COF.

Finally, we analyzed membrane-based CH_4 separation performances of COFs. We performed MD simulations for all COFs and computed gas permeabilities and selectivities for CH_4/H_2 separation, as shown in Figure 5. Since H_2 is weakly adsorbed and has a smaller kinetic radius than CH_4, H_2 diffusion is favored over CH_4 in all COFs. Therefore, we reported the diffusion selectivities of COFs based on H_2. $S_{diff,H_2/CH_4}$ values of COFs mostly dominate their $S_{ads,CH_4/H_2}$, resulting in H_2-selective membranes. H_2/CH_4 adsorption, diffusion, and membrane selectivities of 572 COFs are given in Figure 5a. A trade-off between $S_{ads,H_2/CH_4}$ and $S_{diff,H_2/CH_4}$ is observed since materials with high adsorption selectivities offer low diffusion selectivities and vice versa. For example, in nine of the COFs, diffusion of H_2 was exceptionally faster than that of CH_4, resulting in $S_{diff,H_2/CH_4}$ > 20, as shown by the blue points. Due to very low H_2/CH_4 adsorption selectivities, mediocre $S_{mem,H_2/CH_4}$ were obtained for those COFs (0.01−4.30). The highest membrane selectivities were achieved for COFs with a combination of high $S_{ads,H_2/CH_4}$ (>0.4) and mediocre $S_{diff,H_2/CH_4}$ (>7). For 223 COFs, high CH_4/H_2 adsorption selectivities dominated the H_2/CH_4 diffusion selectivities, leading to CH_4-selective membranes ($S_{mem,CH_4/H_2}$ > 1). Interestingly, 12 of those COFs were offering high CH_4/H_2 adsorption selectivities (31.1 < $S_{ads,CH_4/H_2}$ < 102.7) and diffusion selectivities close to 1 (0.25 < $S_{diff,CH_4/H_2}$ < 0.70), leading to high CH_4/H_2 membrane selectivities (10.4 < $S_{mem,CH_4/H_2}$ < 70.3). Therefore, these 12 COFs can be used as CH_4-selective membranes for separating CH_4/H_2 mixtures.

Gas permeabilities of 572 COFs are given as a function of their membrane selectivities in Figure 5b. H_2/CH_4 separation metrics for MOF membranes computed at infinite dilution from our previous work[85] and Robeson's upper bound,[86] which represents the performance limit of polymeric membranes, were also included in Figure 5b for comparison of COFs with MOFs and polymers. We extended the upper bound for permeabilities that are out of the reach of polymeric membranes. H_2/CH_4 membrane selectivities and H_2 permeabilities of COFs were in the range of 0.01−4.30 and 4.6 × 10^3−1.2 × 10^6 Barrer, respectively. We observed that P_{H_2} values of COFs increase as porosities of COFs increase. This is due to the high self-diffusivity of H_2 in large pore spaces. Interestingly, $S_{mem,H_2/CH_4}$ values of COFs also increase as a function of their porosities, which can be attributed to the low $S_{ads,CH_4/H_2}$ achieved for COFs with high porosities. Thus, we conclude that COFs with high porosities are promising membrane candidates for separation of H_2 from CH_4. The top 10 COF membranes having P_{H_2} > 7.5 × 10^5 Barrer together with the highest membrane selectivities (2.93−4.14) for selective separation of H_2 from CH_4 are displayed in Figure 5. As expected, all of the top COF membranes have high

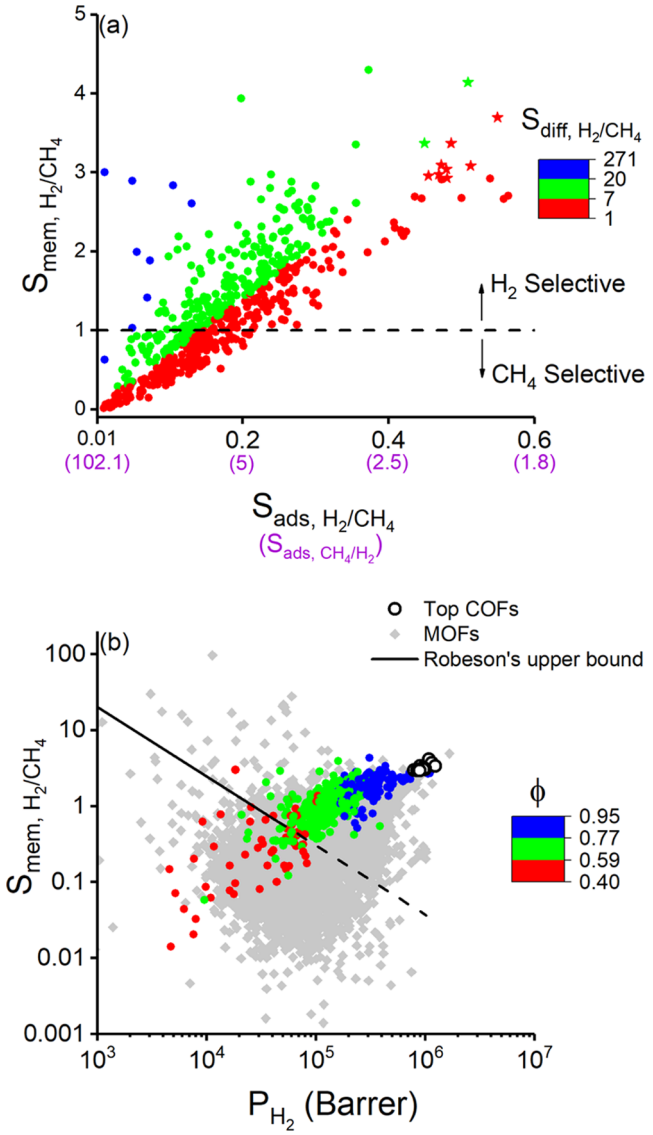

Figure 5. (a) Calculated membrane, diffusion, and adsorption selectivities of 572 COFs at 1 bar. Hollow circles represent the top COF membranes identified for H_2/CH_4 separation. $S_{ads,CH_4/H_2}$ of COFs are provided in purple under the *x*-axis. (b) H_2 permeabilities and H_2/CH_4 membrane selectivities of COFs calculated at 1 bar along with Robeson's upper bound.[86] Colors represent the porosities of COFs. Membrane-based H_2/CH_4 separation performances of 4240 MOFs obtained from our previous work are given in gray diamonds for comparison.[85]

https://doi.org/10.1021/acs.iecr.1c01742
Ind. Eng. Chem. Res. 2021, 60, 12999−13012

porosities (>0.92) and large pore sizes (LCD > 17.5 Å). Many COFs in Figure 5b were observed to surpass Robeson's upper bound, indicating that COFs can outperform polymeric membranes. When compared with MOF membranes, COF membranes are shown to offer lower $S_{mem,H_2/CH_4}$; however, large pore sizes and high porosities of COFs allow them to achieve high H_2 permeabilities. It is also important to note that the membrane properties of MOFs were computed for single-component gases at the infinite dilution condition without considering any gas−gas interactions, and therefore, we can conclude that COFs have comparable and even better membrane-based H_2/CH_4 separation potentials than MOFs.

C_2H_6/CH_4 and N_2/CH_4 separation potentials of the top 10 COFs identified for H_2/CH_4 separation are given in Figure S10. N_2 permeabilities of COFs were observed to be high (1.9×10^5−2.7×10^5 Barrer); however, all 10 COFs were identified to be unselective materials since their $S_{mem,N_2/CH_4}$ values are between 0.66 and 0.87. This is attributed to the similar kinetic diameters of both gases (σ_{N_2} = 3.6 Å, σ_{CH_4} = 3.8 Å)[87] and the very large pores of the COFs, which result in similar self-diffusivities for N_2 and CH_4 in these COFs. Therefore, with respect to the data obtained from the 10 COFs investigated, we concluded that COF membranes are not proper materials for selective N_2/CH_4 separation. COF membranes could achieve very high C_2H_6 permeabilities (1.9×10^5−3.2×10^5 Barrer) for C_2H_6/CH_4 separation, which is higher than the unary C_2H_6 permeability of zeolite MFI membranes experimentally measured at 298 K and 1 bar (2340 GPU corresponding to 1.9×10^3 Barrer).[88] Although COFs could also offer higher C_2H_6/CH_4 membrane selectivities (0.63−1.19) than zeolite MFI (ideal selectivity: 0.57), these selectivities are still very low for selective separation of C_2H_6 from CH_4. Overall, COF membranes were found to offer strong potential only for CH_4/H_2 separation among all separations considered in this study.

4. CONCLUSIONS

In this work, GCMC and MD simulations were performed to reveal the potentials of 572 COFs for both adsorption- and membrane-based CH_4 separation from H_2, N_2, and C_2H_6. Adsorption properties of COFs for equimolar CH_4/H_2, CH_4/N_2, and C_2H_6/CH_4 mixture separations were calculated for VSA and PSA processes. PSA-based separation was found to be preferable for all of the mixtures due to the high working capacities of COFs. The top 10 COF adsorbents having R% > 85% were identified according to their APSs, which outperform traditional adsorbents, zeolites, activated carbon, and mesoporous carbon, for all of the mixture separations considered in this work, indicating that COFs have the potential to replace traditional materials for CH_4 purification. Structure−performance relations revealed that COFs with PLDs < 10 Å are promising adsorbents for CH_4 separation. Moreover, COFs with low porosities (<0.6) are observed to have the best separation potential for VSA- and PSA-based CH_4/H_2 separation, whereas COFs with high porosities (>0.8) are found to be the best materials for PSA-based C_2H_6/CH_4 separation. Among the top COFs, COF-303, COF-300, and PZ-COF2 were found to be common materials for PSA-based CH_4/H_2 and CH_4/N_2 separations and VSA-based C_2H_6/CH_4 separation. DFT calculations were carried out for these three common top materials to investigate the adsorption dynamics of CH_4, H_2, N_2, and C_2H_6. The binding energies of gases obtained from DFT calculations were found to be in the order of C_2H_6 > CH_4 > N_2 > H_2, in accordance with the results of GCMC simulations. For the first time, we applied NICS as an aromaticity criterion to COFs to determine the dependency of adsorption strength of the gases on the strength of aromaticity of the rings on the linkers. We showed that introducing multiple aromatic fragments to the linkers and increasing the extent of aromaticity of the rings in the linkers result in stronger adsorption of C_2H_6 and CH_4, whereas N_2 and H_2 are not directly affected by the aromaticity degree of the rings. Therefore, calculated NICS indexes may guide experimentalists for the design of new COFs with improved CH_4 and C_2H_6 selectivities over N_2 and H_2. MD simulations were performed to assess membrane-based H_2/CH_4 separation performances of COFs. Results showed that there is a trade-off between $S_{ads,H_2/CH_4}$ and $S_{diff,H_2/CH_4}$ values of COFs and COF membranes can achieve high H_2 permeabilities (4.69×10^3−1.24×10^6 Barrer) and mediocre selectivities (0.01−4.3), outperforming traditional polymers and high-performing MOFs for membrane-based separation of H_2 from CH_4. Moreover, 12 COFs were shown to have high $S_{mem,CH_4/H_2}$ (10.4−70.3), demonstrating the potential of COFs to act as CH_4-selective membranes. The top 10 COF membranes identified for H_2/CH_4 separation were found to be unselective for N_2/CH_4 and C_2H_6/CH_4 separations, but they can achieve higher N_2 and C_2H_6 permeabilities than polymer and zeolite membranes. In conclusion, COFs were shown to be promising in PSA-based CH_4/N_2 and C_2H_6/CH_4 separations, outperforming commercial adsorbents, and in membrane-based CH_4/H_2 separation, exceeding the performance limit of polymers. The results obtained from this multiscale computational study will open new horizons for the selection and design of high-performance COFs as an emerging class of porous materials for CH_4 purification applications.

■ ASSOCIATED CONTENT

Supporting Information

The Supporting Information is available free of charge at https://pubs.acs.org/doi/10.1021/acs.iecr.1c01742.

Comparison of C_2H_6 and CH_4 adsorption isotherms obtained from GCMC simulations with experimental results; selectivities and ΔQ_{st} of COFs for CH_4/H_2 and CH_4/N_2 mixtures at 1 bar; comparison of CH_4/N_2 selectivities of COFs with and without considering electrostatic interactions between COF atoms and N_2; lists of the top 10 COF adsorbents for CH_4/H_2, CH_4/N_2, and C_2H_6/CH_4 separations; structural representation of the top COF adsorbents for CH_4/H_2, CH_4/N_2, and C_2H_6/CH_4 separation applications; APSs of COFs as a function of their porosities and PLDs for CH_4/H_2 and CH_4/N_2 separations at VSA conditions; 3D representations of the interactions between the most favorable adsorption sites on the top three COFs and CH_4, C_2H_6, N_2, and H_2; adsorption snapshots of C_2H_6, CH_4, N_2, and H_2 in COF-300; $P_{C_2H_6/CH_4}$, P_{N_2/CH_4}, $S_{mem,C_2H_6/CH_4}$, and $S_{mem,N_2/CH_4}$ of the COF membranes; Cartesian coordinates of cluster models and gas molecules calculated at the B3LYP-D2/6-31G* level of theory (PDF)

https://doi.org/10.1021/acs.iecr.1c01742
Ind. Eng. Chem. Res. 2021, 60, 12999−13012

AUTHOR INFORMATION

Corresponding Author

Seda Keskin − *Department of Chemical and Biological Engineering, Koc University, 34450 Istanbul, Turkey;* orcid.org/0000-0001-5968-0336; Phone: +90 (212) 338-1362; Email: skeskin@ku.edu.tr

Authors

Omer Faruk Altundal − *Department of Chemical and Biological Engineering, Koc University, 34450 Istanbul, Turkey*

Zeynep Pinar Haslak − *Department of Chemical and Biological Engineering, Koc University, 34450 Istanbul, Turkey;* orcid.org/0000-0002-2850-9816

Complete contact information is available at: https://pubs.acs.org/10.1021/acs.iecr.1c01742

Notes

The authors declare no competing financial interest.

ACKNOWLEDGMENTS

S.K. acknowledges the ERC-2017-Starting Grant. This study has received funding from the European Research Council (ERC) under the European Union's Horizon 2020 research and innovation program (ERC-2017-Starting Grant, grant agreement No. 756489-COSMOS).

REFERENCES

(1) Litvinenko, V. The Role of Hydrocarbons in the Global Energy Agenda: The Focus on Liquefied Natural Gas. *Resources* **2020**, *9*, No. 59.

(2) Ponraj, Y. K.; Borah, B. Separation of Methane from Ethane and Propane by Selective Adsorption and Diffusion in MOF Cu-BTC: A Molecular Simulation Study. *J. Mol. Graphics Modell.* **2020**, *97*, No. 107574.

(3) Bhadra, S.; Farooq, S. Separation of Methane−Nitrogen Mixture by Pressure Swing Adsorption for Natural Gas Upgrading. *Ind. Eng. Chem. Res.* **2011**, *50*, 14030−14045.

(4) Knaebel, S. P.; Ko, D.; Biegler, L. T. Simulation and Optimization of a Pressure Swing Adsorption System: Recovering Hydrogen from Methane. *Adsorption* **2005**, *11*, 615−620.

(5) Olajossy, A.; Gawdzik, A.; Budner, Z.; Dula, J. Methane Separation from Coal Mine Methane Gas by Vacuum Pressure Swing Adsorption. *Chem. Eng. Res. Des.* **2003**, *81*, 474−482.

(6) Lin, Y.; Kong, C.; Zhang, Q.; Chen, L. Metal-Organic Frameworks for Carbon Dioxide Capture and Methane Storage. *Adv. Energy Mater.* **2017**, *7*, No. 1601296.

(7) Alonso, A.; Moral-Vico, J.; Markeb, A. A.; Busquets-Fité, M.; Komilis, D.; Puntes, V.; Sánchez, A.; Font, X. Critical Review of Existing Nanomaterial Adsorbents to Capture Carbon Dioxide and Methane. *Sci. Total Environ.* **2017**, *595*, 51−62.

(8) Jiang, J. Molecular Simulations in Metal−Organic Frameworks for Diverse Potential Applications. *Mol. Simul.* **2014**, *40*, 516−536.

(9) Deng, H.; Grunder, S.; Cordova, K. E.; Valente, C.; Furukawa, H.; Hmadeh, M.; Gándara, F.; Whalley, A. C.; Liu, Z.; Asahina, S.; et al. Large-Pore Apertures in a Series of Metal-Organic Frameworks. *Science* **2012**, *336*, 1018−1023.

(10) Daglar, H.; Gulbalkan, H. C.; Avci, G.; Aksu, G. O.; Altundal, O. F.; Altintas, C.; Erucar, I.; Keskin, S. Effect of MOF Database Selection on the Assessment of Gas Storage and Separation Potentials of MOFs. *Angew. Chem., Int. Ed.* **2021**, *60*, 7828−7837.

(11) Daglar, H.; Keskin, S. Recent Advances, Opportunities, and Challenges in High-Throughput Computational Screening of MOFs for Gas Separations. *Coord. Chem. Rev.* **2020**, *422*, No. 213470.

(12) Belmabkhout, Y.; Bhatt, P. M.; Adil, K.; Pillai, R. S.; Cadiau, A.; Shkurenko, A.; Maurin, G.; Liu, G.; Koros, W. J.; Eddaoudi, M. Natural Gas Upgrading Using a Fluorinated MOF with Tuned H_2S and CO_2 Adsorption Selectivity. *Nat. Energy* **2018**, *3*, 1059−1066.

(13) Qiao, Z.; Xu, Q.; Jiang, J. High-Throughput Computational Screening of Metal-Organic Framework Membranes for Upgrading of Natural Gas. *J. Membr. Sci.* **2018**, *551*, 47−54.

(14) Li, J.-R.; Kuppler, R. J.; Zhou, H.-C. Selective Gas Adsorption and Separation in Metal−Organic Frameworks. *Chem. Soc. Rev.* **2009**, *38*, 1477−1504.

(15) Lin, R.-B.; Xiang, S.; Xing, H.; Zhou, W.; Chen, B. Exploration of Porous Metal−Organic Frameworks for Gas Separation and Purification. *Coord. Chem. Rev.* **2019**, *378*, 87−103.

(16) Basdogan, Y.; Sezginel, K. B.; Keskin, S. Identifying Highly Selective Metal Organic Frameworks for CH_4/H_2 Separations Using Computational Tools. *Ind. Eng. Chem. Res.* **2015**, *54*, 8479−8491.

(17) Moghadam, P. Z.; Li, A.; Wiggin, S. B.; Tao, A.; Maloney, A. G.; Wood, P. A.; Ward, S. C.; Fairen-Jimenez, D. Development of a Cambridge Structural Database Subset: A Collection of Metal−Organic Frameworks for Past, Present, and Future. *Chem. Mater.* **2017**, *29*, 2618−2625.

(18) Han, S.; Huang, Y.; Watanabe, T.; Dai, Y.; Walton, K. S.; Nair, S.; Sholl, D. S.; Meredith, J. C. High-Throughput Screening of Metal−Organic Frameworks for CO_2 Separation. *ACS Comb. Sci.* **2012**, *14*, 263−267.

(19) Bobbitt, N. S.; Chen, J.; Snurr, R. Q. High-Throughput Screening of Metal−Organic Frameworks for Hydrogen Storage at Cryogenic Temperature. *J. Phys. Chem. C* **2016**, *120*, 27328−27341.

(20) Altintas, C.; Avci, G.; Daglar, H.; Azar, A. N. V.; Erucar, I.; Velioglu, S.; Keskin, S. An Extensive Comparative Analysis of Two MOF Databases: High-Throughput Screening of Computation-Ready MOFs for CH_4 and H_2 Adsorption. *J. Mater. Chem. A* **2019**, *7*, 9593−9608.

(21) Altintas, C.; Keskin, S. Computational Screening of MOFs for C_2H_6/C_2H_4 and C_2H_6/CH_4 Separations. *Chem. Eng. Sci.* **2016**, *139*, 49−60.

(22) Wu, D.; Wang, C.; Liu, B.; Liu, D.; Yang, Q.; Zhong, C. Large-Scale Computational Screening of Metal-Organic Frameworks for CH_4/H_2 Separation. *AIChE J.* **2012**, *58*, 2078−2084.

(23) Altintas, C.; Erucar, I.; Keskin, S. High-Throughput Computational Screening of the Metal Organic Framework Database for CH_4/H_2 Separations. *ACS Appl. Mater. Interfaces* **2018**, *10*, 3668−3679.

(24) Yan, T.; Lan, Y.; Liu, D.; Yang, Q.; Zhong, C. Large-Scale Screening and Design of Metal−Organic Frameworks for CH_4/N_2 Separation. *Chem. - Asian J.* **2019**, *14*, 3688−3693.

(25) Ponraj, Y. K.; Borah, B. High-Throughput Computational Screening of Metal−Organic Frameworks for the Separation of Methane from Ethane and Propane. *J. Phys. Chem. C* **2021**, *125*, 1839−1854.

(26) Altintas, C.; Keskin, S. Molecular Simulations of MOF Membranes for Separation of Ethane/Ethene and Ethane/Methane Mixtures. *RSC Adv.* **2017**, *7*, 52283−52295.

(27) Erucar, I.; Keskin, S. Computational Assessment of MOF Membranes for CH_4/H_2 Separations. *J. Membr. Sci.* **2016**, *514*, 313−321.

(28) Song, Y.; Sun, Q.; Aguila, B.; Ma, S. Opportunities of Covalent Organic Frameworks for Advanced Applications. *Adv. Sci.* **2019**, *6*, No. 1801410.

(29) Díaz, U.; Corma, A. Ordered Covalent Organic Frameworks, COFs and PAFs. From Preparation to Application. *Coord. Chem. Rev.* **2016**, *311*, 85−124.

(30) Feng, X.; Ding, X.; Jiang, D. Covalent Organic Frameworks. *Chem. Soc. Rev.* **2012**, *41*, 6010−6022.

(31) Waller, P. J.; Gándara, F.; Yaghi, O. M. Chemistry of Covalent Organic Frameworks. *Acc. Chem. Res.* **2015**, *48*, 3053−3063.

(32) Ding, S.-Y.; Wang, W. Covalent Organic Frameworks (COFs): From Design to Applications. *Chem. Soc. Rev.* **2013**, *42*, 548−568.

(33) El-Kaderi, H. M.; Hunt, J. R.; Mendoza-Cortés, J. L.; Côté, A. P.; Taylor, R. E.; O'Keeffe, M.; Yaghi, O. M. Designed Synthesis of 3D Covalent Organic Frameworks. *Science* **2007**, *316*, 268−272.

(34) Yang, Z.; Cao, D. Effect of Li Doping on Diffusion and Separation of Hydrogen and Methane in Covalent Organic Frameworks. *J. Phys. Chem. C* **2012**, *116*, 12591−12598.
(35) Tong, M.; Yang, Q.; Zhong, C. Computational Screening of Covalent Organic Frameworks for CH_4/H_2, CO_2/H_2 and CO_2/CH_4 Separations. *Microporous Mesoporous Mater.* **2015**, *210*, 142−148.
(36) Tong, M. M.; Lan, Y. S.; Yang, Q. Y.; Zhong, C. L. Exploring the Structure-Property Relationships of Covalent Organic Frameworks for Noble Gas Separations. *Chem. Eng. Sci.* **2017**, *168*, 456−464.
(37) Yan, T.; Lan, Y.; Tong, M.; Zhong, C. Screening and Design of Covalent Organic Framework Membranes for CO_2/CH_4 Separation. *ACS Sustainable Chem. Eng.* **2019**, *7*, 1220−1227.
(38) Ongari, D.; Yakutovich, A. V.; Talirz, L.; Smit, B. Building a Consistent and Reproducible Database for Adsorption Evaluation in Covalent−Organic Frameworks. *ACS Cent. Sci.* **2019**, *5*, 1663−1675.
(39) Deeg, K. S.; Damasceno Borges, D.; Ongari, D.; Rampal, N.; Talirz, L.; Yakutovich, A. V.; Huck, J. M.; Smit, B. In Silico Discovery of Covalent Organic Frameworks for Carbon Capture. *ACS Appl. Mater. Interfaces* **2020**, *12*, 21559−21568.
(40) Altundal, O. F.; Altintas, C.; Keskin, S. Can COFs Replace MOFs in Flue Gas Separation? High-Throughput Computational Screening of COFs for CO_2/N_2 Separation. *J. Mater. Chem. A* **2020**, *8*, 14609−14623.
(41) Aksu, G. O.; Daglar, H.; Altintas, C.; Keskin, S. Computational Selection of High-Performing Covalent Organic Frameworks for Adsorption and Membrane-Based CO_2/H_2 Separation. *J. Phys. Chem. C* **2020**, *124*, 22577−22590.
(42) Willems, T. F.; Rycroft, C. H.; Kazi, M.; Meza, J. C.; Haranczyk, M. Algorithms and Tools for High-Throughput Geometry-Based Analysis of Crystalline Porous Materials. *Microporous Mesoporous Mater.* **2012**, *149*, 134−141.
(43) Junior, M. J. C.; Wang, Y.; Wu, X.; Cai, W. Computational Screening of Metal-Organic Frameworks with Open Copper Sites for Hydrogen Purification. *Int. J. Hydrogen Energy* **2020**, *45*, 27320−27330.
(44) Javani, R.; Maghsoudi, H.; Darvishi Gilan, S.; Majidpour, M. Study on Adsorption Performance of Different Adsorbents in Nitrogen/Methane Separation. *Sep. Sci. Technol.* **2020**, 1−16.
(45) Guo, H.-c.; Shi, F.; Ma, Z.-f.; Liu, X.-q. Molecular Simulation for Adsorption and Separation of CH_4/H_2 in Zeolitic Imidazolate Frameworks. *J. Phys. Chem. C* **2010**, *114*, 12158−12165.
(46) Guo, H.; Shi, F.; Ma, Z.; Liu, X. Simulation of Separation of C_2H_6 from CH_4 Using Zeolitic Imidazolate Frameworks. *Mol. Simul.* **2014**, *40*, 349−360.
(47) Dubbeldam, D.; Calero, S.; Ellis, D. E.; Snurr, R. Q. Raspa: Molecular Simulation Software for Adsorption and Diffusion in Flexible Nanoporous Materials. *Mol. Simul.* **2016**, *42*, 81−101.
(48) Karavias, F.; Myers, A. L. Isosteric Heats of Multicomponent Adsorption: Thermodynamics and Computer Simulations. *Langmuir* **1991**, *7*, 3118−3126.
(49) Peng, D.-Y.; Robinson, D. B. A New Two-Constant Equation of State. *Ind. Eng. Chem. Fundam.* **1976**, *15*, 59−64.
(50) Tee, L. S.; Gotoh, S.; Stewart, W. E. Molecular Parameters for Normal Fluids. Lennard-Jones 12-6 Potential. *Ind. Eng. Chem. Fundam.* **1966**, *5*, 356−363.
(51) Goldstein, H.; Poole, C.; Safko, J. *Classical Mechanics*; American Association of Physics Teachers, 2002.
(52) Ewald, P. P. Die Berechnung Optischer Und Elektrostatischer Gitterpotentiale. *Ann. Phys.* **1921**, *369*, 253−287.
(53) Buch, V. Path Integral Simulations of Mixed Para-D_2 and Ortho-D_2 Clusters: The Orientational Effects. *J. Chem. Phys.* **1994**, *100*, 7610−7629.
(54) Eggimann, B. L.; Sunnarborg, A. J.; Stern, H. D.; Bliss, A. P.; Siepmann, J. I. An Online Parameter and Property Database for the Trappe Force Field. *Mol. Simul.* **2014**, *40*, 101−105.
(55) Martin, M. G.; Siepmann, J. I. Transferable Potentials for Phase Equilibria. 1. United-Atom Description of N-Alkanes. *J. Phys. Chem. B* **1998**, *102*, 2569−2577.
(56) Murthy, C.; Singer, K.; Klein, M.; McDonald, I. Pairwise Additive Effective Potentials for Nitrogen. *Mol. Phys.* **1980**, *41*, 1387−1399.
(57) Mayo, S. L.; Olafson, B. D.; Goddard, W. A. Dreiding: A Generic Force Field for Molecular Simulations. *J. Phys. Chem. A* **1990**, *94*, 8897−8909.
(58) Furukawa, H.; Yaghi, O. M. Storage of Hydrogen, Methane, and Carbon Dioxide in Highly Porous Covalent Organic Frameworks for Clean Energy Applications. *J. Am. Chem. Soc.* **2009**, *131*, 8875−8883.
(59) Becke, A. D. Density-Functional Thermochemistry. Iii. The Role of Exact Exchange. *J. Chem. Phys.* **1993**, *98*, 5648−5652.
(60) Lee, C.; Yang, W.; Parr, R. G. Development of the Colle-Salvetti Correlation-Energy Formula into a Functional of the Electron Density. *Phys. Rev. B* **1988**, *37*, 785−789.
(61) Grimme, S.; Antony, J.; Ehrlich, S.; Krieg, H. A Consistent and Accurate ab Initio Parametrization of Density Functional Dispersion Correction (DFT-D) for the 94 Elements H-Pu. *J. Chem. Phys.* **2010**, *132*, No. 154104.
(62) Frisch, M. J.; Trucks, G. W.; Schlegel, H. B.; Scuseria, G. E.; Robb, M. A.; Cheeseman, J. R.; Scalmani, G.; Barone, V.; Petersson, G. A.; Nakatsuji, H.; Li, X.; Caricato, M.; Marenich, A. V.; Bloino, J.; Janesko, B. G.; Gomperts, R.; Mennucci, B.; Hratchian, H. P.; Ortiz, J. V.; Izmaylov, A. F.; Sonnenberg, J. L.; Williams; Ding, F.; Lipparini, F.; Egidi, F.; Goings, J.; Peng, B.; Petrone, A.; Henderson, T.; Ranasinghe, D.; Zakrzewski, V. G.; Gao, J.; Rega, N.; Zheng, G.; Liang, W.; Hada, M.; Ehara, M.; Toyota, K.; Fukuda, R.; Hasegawa, J.; Ishida, M.; Nakajima, T.; Honda, Y.; Kitao, O.; Nakai, H.; Vreven, T.; Throssell, K.; Montgomery, J. A., Jr.; Peralta, J. E.; Ogliaro, F.; Bearpark, M. J.; Heyd, J. J.; Brothers, E. N.; Kudin, K. N.; Staroverov, V. N.; Keith, T. A.; Kobayashi, R.; Normand, J.; Raghavachari, K.; Rendell, A. P.; Burant, J. C.; Iyengar, S. S.; Tomasi, J.; Cossi, M.; Millam, J. M.; Klene, M.; Adamo, C.; Cammi, R.; Ochterski, J. W.; Martin, R. L.; Morokuma, K.; Farkas, O.; Foresman, J. B.; Fox, D. J. *Gaussian 09*, rev. E.01; Gaussian Inc.: Wallingford, CT.
(63) Frenkel, D.; Smit, B. *Understanding Molecular Simulation: From Algorithms to Applications*; Elsevier, 2001; Vol. *1*.
(64) Einstein, A. *Investigations on the Theory of the Brownian Movement*; Courier Corporation, 1956.
(65) Liu, B.; Smit, B. Molecular Simulation Studies of Separation of CO_2/N_2, CO_2/CH_4, and CH_4/N_2 by ZIFs. *J. Phys. Chem. C* **2010**, *114*, 8515−8522.
(66) Gulbalkan, H. C.; Haslak, Z. P.; Altintas, C.; Uzun, A.; Keskin, S. Assessing CH_4/N_2 separation potential of MOFs, COFs, IL/MOF, MOF/Polymer, and COF/Polymer composites. *Chem. Eng. J.* **2022**, *428*, 131239.
(67) Chung, Y. G.; Gómez-Gualdrón, D. A.; Li, P.; Leperi, K. T.; Deria, P.; Zhang, H.; Vermeulen, N. A.; Stoddart, J. F.; You, F.; Hupp, J. T.; et al. In Silico Discovery of Metal-Organic Frameworks for Precombustion CO_2 Capture Using a Genetic Algorithm. *Sci. Adv.* **2016**, *2*, No. e1600909.
(68) Wu, D.; Yang, Q.; Zhong, C.; Liu, D.; Huang, H.; Zhang, W.; Maurin, G. Revealing the Structure−Property Relationships of Metal−Organic Frameworks for CO_2 Capture from Flue Gas. *Langmuir* **2012**, *28*, 12094−12099.
(69) Wilmer, C. E.; Farha, O. K.; Bae, Y.-S.; Hupp, J. T.; Snurr, R. Q. Structure−Property Relationships of Porous Materials for Carbon Dioxide Separation and Capture. *Energy Environ. Sci.* **2012**, *5*, 9849−9856.
(70) Basdogan, Y.; Sezginel, K. B.; Keskin, S. Identifying Highly Selective Metal Organic Frameworks for CH_4/H_2 Separations Using Computational Tools. *Ind. Eng. Chem. Res.* **2015**, *54*, 8479−8491.
(71) Avci, G.; Erucar, I.; Keskin, S. Do New MOFs Perform Better for CO_2 Capture and H_2 Purification? Computational Screening of the Updated MOF Database. *ACS Appl. Mater. Interfaces* **2020**, *12*, 41567−41579.
(72) Pitakbunkate, T.; Blasingame, T.; Moridis, G.; Balbuena, P. Phase Behavior of Methane−Ethane Mixtures in Nanopores. *Ind. Eng. Chem. Res.* **2017**, *56*, 11634−11643.

https://doi.org/10.1021/acs.iecr.1c01742
Ind. Eng. Chem. Res. 2021, 60, 12999−13012

(73) Ma, T.; Kapustin, E. A.; Yin, S. X.; Liang, L.; Zhou, Z.; Niu, J.; Li, L.-H.; Wang, Y.; Su, J.; Li, J.; et al. Single-Crystal X-Ray Diffraction Structures of Covalent Organic Frameworks. *Science* **2018**, *361*, 48−52.
(74) Delgado, J. A.; Águeda, V.; Uguina, M.; Sotelo, J.; Brea, P.; Grande, C. A. Adsorption and Diffusion of H_2, CO, CH_4, and CO_2 in BPL Activated Carbon and 13X Zeolite: Evaluation of Performance in Pressure Swing Adsorption Hydrogen Purification by Simulation. *Ind. Eng. Chem. Res.* **2014**, *53*, 15414−15426.
(75) Jensen, N. K.; Rufford, T. E.; Watson, G.; Zhang, D. K.; Chan, K. I.; May, E. F. Screening Zeolites for Gas Separation Applications Involving Methane, Nitrogen, and Carbon Dioxide. *J. Chem. Eng. Data* **2012**, *57*, 106−113.
(76) Hosseinpour, S.; Fatemi, S.; Mortazavi, Y.; Gholamhoseini, M.; Ravanchi, M. T. Performance of CaX Zeolite for Separation of C_2H_6, C_2H_4, and CH_4 by Adsorption Process; Capacity, Selectivity, and Dynamic Adsorption Measurements. *Sep. Sci. Technol.* **2010**, *46*, 349−355.
(77) Schleyer, P. V. R.; Maerker, C.; Dransfeld, A.; Jiao, H.; Van Eikema Hommes, N. J. R. Nucleus-Independent Chemical Shifts: A Simple and Efficient Aromaticity Probe. *J. Am. Chem. Soc.* **1996**, *118*, 6317−6318.
(78) Stanger, A. Nucleus-Independent Chemical Shifts (Nics): Distance Dependence and Revised Criteria for Aromaticity and Antiaromaticity. *J. Org. Chem.* **2006**, *71*, 883−893.
(79) Gomes, J. A. N. F.; Mallion, R. B. Aromaticity and Ring Currents. *Chem. Rev.* **2001**, *101*, 1349−1384.
(80) Lazzeretti, P. Ring Currents. *Prog. Nucl. Magn. Reson. Spectrosc.* **2000**, *36*, 1−88.
(81) Lazzeretti, P. Assessment of Aromaticity via Molecular Response Properties. *Phys. Chem. Chem. Phys.* **2004**, *6*, 217−223.
(82) Schleyer, P. v. R.; Jiao, H.; Hommes, N. J. R. vE.; Malkin, V. G.; Malkina, O. L. An Evaluation of the Aromaticity of Inorganic Rings: Refined Evidence from Magnetic Properties. *J. Am. Chem. Soc.* **1997**, *119*, 12669−12670.
(83) Olney, T. N.; Cann, N. M.; Cooper, G.; Brion, C. E. Absolute Scale Determination for Photoabsorption Spectra and the Calculation of Molecular Properties Using Dipole Sum-Rules. *Chem. Phys.* **1997**, *223*, 59−98.
(84) Levitt, M.; Perutz, M. F. Aromatic Rings Act as Hydrogen Bond Acceptors. *J. Mol. Biol.* **1988**, *201*, 751−754.
(85) Altintas, C.; Avci, G.; Daglar, H.; Gulcay, E.; Erucar, I.; Keskin, S. Computer Simulations of 4240 MOF Membranes for H_2/CH_4 Separations: Insights into Structure−Performance Relations. *J. Mater. Chem. A* **2018**, *6*, 5836−5847.
(86) Robeson, L. M. The Upper Bound Revisited. *J. Membr. Sci.* **2008**, *320*, 390−400.
(87) Tagliabue, M.; Farrusseng, D.; Valencia, S.; Aguado, S.; Ravon, U.; Rizzo, C.; Corma, A.; Mirodatos, C. Natural Gas Treating by Selective Adsorption: Material Science and Chemical Engineering Interplay. *Chem. Eng. J.* **2009**, *155*, 553−566.
(88) Min, B.; Korde, A.; Yang, S.; Kim, Y.; Jones, C. W.; Nair, S. Separation of C2−C4 Hydrocarbons from Methane by Zeolite MFI Hollow Fiber Membranes Fabricated from 2D Nanosheets. *AIChE J.* **2021**, *67*, No. e17048.

https://doi.org/10.1021/acs.iecr.1c01742
Ind. Eng. Chem. Res. 2021, 60, 12999−13012